Probing Hot and Dense Laser-Induced Plasmas with Ultrafast XUV Pulses

S. Dobosz,[1] G. Doumy,[1] H. Stabile,[1] P. D'Oliveira,[1] P. Monot,[1] F. Réau,[1] S. Hüller,[2] and Ph. Martin[1]

[1]*Service des Photons, Atomes et Molécules, Commissariat à l'Energie Atomique, DSM/DRECAM, CEN Saclay, 91191 Gif sur Yvette, France*

[2]*Centre de Physique Théorique, Ecole Polytechnique, CNRS UMR 7644, F-91128, Palaiseau, France*

(Received 11 March 2005; published 5 July 2005)

In this Letter, we demonstrate the instantaneous creation of a hot solid-density plasma generated by focusing an intense femtosecond, high temporal contrast laser on an ultrathin foil (100 nm) in the 10^{18} W/cm^2 intensity range. The use of high-order harmonics generated in a gas jet, providing a probe beam of sufficiently short wavelengths to penetrate such a medium, enables the study of the dynamics of this plasma on the 100 fs time scale. The comparison of the transmission of two successive harmonics permits us to determine the electronic density and the temperature with accuracies better than 15%, never achieved up to this date in the regime of laser pulses at relativistic intensity.

DOI: 10.1103/PhysRevLett.95.025001 PACS numbers: 52.50.Jm, 52.70.Kz

In the past years, thanks to the development of both ultraintense and ultrahigh-contrast lasers, the study of solids in yet inaccessible matter states, namely, hot dense matter, has become possible. In this context, a number of fundamental processes have been discussed, such as vacuum heating [1], relativistic harmonics generation [2,3], or penetration of ultraintense light into dense matter through the anomalous skin effect, hole boring, or self induced transparency [4].

Recently a strong growing interest has appeared for thin foils as efficient targets for the generation of multi-MeV ions [5,6] and collimated proton beams [7].

Investigations of the dynamics of plasmas at solid density suffer from the complexity to set up efficient diagnostics and also from the high sensitivity of thin foils to the laser pedestal causing prematurely its expansion.

In contrast to low-density plasmas, dense plasmas cannot be studied using optical probes in the visible domain. Light with a given wavelength λ will be reflected once the electron density exceeds the critical density n_{cr} (cm^{-3}) = 1.1×10^{21} cm$^{-3}/[\lambda\ (\mu\text{m})]^2$. In addition, light is refracted for even slightly lower density if the medium exhibits a sharp density gradient. Large deflection angles imply significant spatial blurring and reduce the spatial resolution. These two adverse effects (reflection and refraction) can be significantly reduced by using a short wavelength probe. This explains why XUV techniques provide the essential means of probing dense samples in a wide range of scientific endeavors such as inertial confinement fusion, laser-plasma interaction physics, as well as high temperature and high density laboratory plasmas for astrophysics. Based on XUV wavelengths, a lot of time-dependent techniques have been developed going from the nanosecond [8] to the picosecond [9,10] time scale. Recently, using an x-ray laser, a picosecond imagery interferometric method has been demonstrated and utilized to provide two-dimensional maps of overdense plasmas on the picosecond time scale [11].

Subpicosecond temporal resolution requires ultrashort duration sources. A pioneering study using high-order harmonics of laser light generated in a gas jet [12] was done by Theobald *et al.* [13]. By measuring the harmonics absorption, they demonstrated for the first time the relevance of this source, allowing for the determination of the electron density and temperature of a plasma generated on a thin foil in the 10^{14} W/cm^2 range using a 0.7 ps, 248 nm KrF laser.

To produce solid-density plasmas in the high intensity range, it is necessary to improve significantly the contrast ratio of the laser pulse. Indeed, because of either imperfect compression or amplified spontaneous emission (ASE), background light accompanies the short intense pulse at the focus. With peak intensities around 10^{18} W/cm^2 and a typical contrast ratio of 10^6, the pedestal alone is sufficiently powerful to create a preplasma well before the arrival of the main pulse. As a consequence, the high intensity part of the laser pulse interacts with a plasma with a non-negligible density gradient instead of a quite sharp interface between vacuum and solid-density matter. Hence the laser energy is deposited closer to the critical density region of a long scale length plasma rather than directly at solid density, corrupting the direct instantaneous heating of the matter at solid density. Recently, significant progress in the ASE suppression have been accomplished with the so-called plasma mirror (PM) [14,15]. This is an optical switch, triggered by the main pulse itself. The laser beam is sent on a low reflectivity vacuum-dielectric interface which transmits most of the pedestal, whereas the main pulse is reflected by the self generated overcritical plasma. This tool has been used to observe well collimated high-order harmonics from massive solid targets [16]. However, although the experimental observations strongly indicated that the preplasma was properly suppressed before the main interaction, a direct demonstration of its absence was not achieved.

In this work, using a PM, we probe a solid-density plasma produced by the interaction of a relativistic highly contrasted laser pulse with an ultrathin foil by measuring *the absolute transmission* (in percent of the incident beam) of high-order harmonics generated in a gas jet. We will clearly show by imaging the interaction zone, using as a probe a near infrared (800 nm) pulse, that the reflection/refraction of the probe occurs only *after* the passage of the main pulse providing the evidence that no overdense plasma is generated before the main pulse. In a second step, by using XUV wavelengths, we will *measure* the actual electronic density and thus prove that the plasma is indeed created at the solid density. The subsequent evolution is then followed on the picosecond time scale and the confrontation with hydrodynamic simulations allows for a determination of the electronic temperature.

In our experiment, the plasma is generated by the main pulse of the UHI10 laser (SLIC facility, Saclay, France), which provides pulses of 600 mJ in 60 fs at 800 nm. The experimental setup is reported in Fig. 1. The laser beam, focused with an $f/6$ off-axis parabola ($f = 500$ mm), is s polarized on the target as well as onto the PM surface in order to maximize the PM reflectivity once triggered. In order to adjust the incident fluence on the PM to about 60 J/cm^2 [15], it is set 12 mm before the focus. Under these conditions, the contrast can be improved by a factor ≥ 200, while keeping a peak reflectivity of 70%. As detailed in [16], the intensity on the target is then as high as 3×10^{17} W/cm^2, with a nanosecond temporal contrast of at least 10^8. The target consists of a 100 nm-thick self-supporting polypropylene foil $(C_3H_6)_n$ with a density of 0.9 g/cm^3. This foil, maintained between two aluminum drilled plates, is moved at each shot to show an intact area.

An auxiliary low-energy IR beam is used to probe the time-dependent target transmission. The beam crosses the foil with an angle of 47° and a time delay line is used to adjust the pump-probe delay. This beam is defocused in order to illuminate a much larger spot (2 mm) than the pump beam waist (50 μm). The transmitted probe beam is imaged in the target plane onto a CCD camera. Since the foil is initially transparent to visible light, any reduction of the probe transmission reveals the creation of a plasma. The temporal synchronization of both pump and probe beams is achieved by using a dielectric plate placed right beneath the foil target by probing the creation of the optical damage induced by the pump (strongly attenuated in order to avoid any influence of the pedestal).

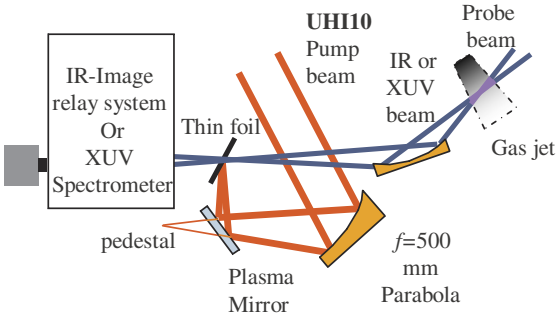

FIG. 1 (color online). Schematic experimental setup. The main 10 TW IR beam is focused onto a thin polypropylene foil. A plasma mirror filtering the laser pedestal is set before the focus. An IR probe beam can be used to image the foil transmission. A gas jet can be inserted to generate high-order harmonics, analyzed after propagation through the foil by an XUV spectrometer.

The evolution of the transmission as a function of the delay between the probe and the pump (the zero delay represents the temporal superposition) is reported in Fig. 2(a)—without the PM—and Fig. 2(b)—with the PM. Without the PM, it appears clearly on the Fig. 2(a) that, 1 ns before the arrival of the main pulse, an opaque zone is already present. This originates from the reflection and/or the refraction of the IR probe on a preplasma. This result is explained by the interaction with the pedestal of the pump pulse, creating on the nanosecond time scale an overcritical plasma evolving insignificantly on the picosecond range.

Figure 2(b) illustrates the role of the PM. Because of the contrast improvement, the energy contained in the ASE is no longer sufficient to ionize the target, so that the plasma is just created around the peak intensity. As discussed in [17], the utilization of a transparent target is also expected to avoid the (neutral) vaporization of the target. The opaque region corresponding to the overcritical plasma evolves significantly on a few picoseconds' time scale and is also the result of the refraction and reflection of the probe.

By using the PM and going to shorter wavelengths, we should now be able to measure directly the initial electronic density and follow its evolution. The corresponding setup is presented in Fig. 1. The secondary IR beam of UHI10 laser is focused with a 1 m focal length lens in a pulsed argon gas jet to generate harmonics. They are then

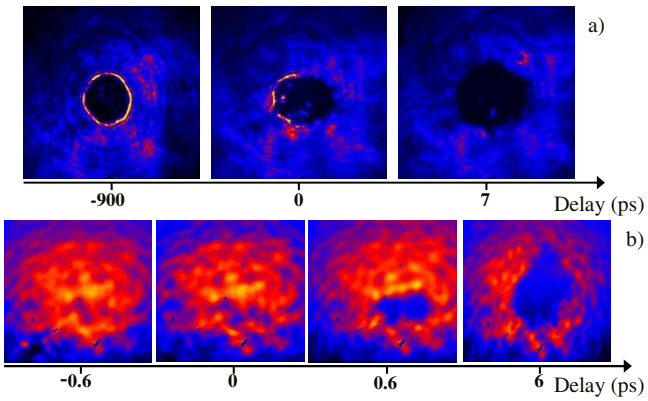

FIG. 2 (color online). Transmission of an 800 nm probe through a 100 nm thin foil with (up) and without (down) the presence of a preplasma caused by ASE.

focused onto the target by a toroidal mirror. The harmonics, being s polarized with respect to the target at an incident angle of 47°, follow exactly the same path as the IR beam in the previous set of experiments. Harmonics transmitted through the plasma are then separated in a spectrometer composed of a toroidal mirror and a gold coated grating (700 lines/mm). The detector is an ensemble of two microchannel plates coupled to a phosphor screen. The spectrum is then imaged onto an 8 bit CCD camera. We measured that, without pump shot, the absorption is total through the foil for the H19 and H21.

Since the imaginary part of the plasma refractive index is a function of both the electronic density and the temperature, the *absolute* transmission measurement of two harmonics results in the determination of this couple of parameters. In order to obtain the best accuracy, we selected two neighboring specific harmonics, chosen so that their corresponding critical densities enclose the maximum expected density reached during the experiment. In the high intensity regime reached herein, the target is expected to be fully ionized, leading to a maximum 3.1×10^{23} cm^{-3} electronic density. Taking into account the angle of incidence, the critical densities $n_{\mathrm{cr}} = 1.1 \times 10^{21}/(\lambda^2 \times \cos^2\theta)$ of H19 and H21, respectively, 2.9×10^{23} and 3.5×10^{23}, are found to enclose satisfactorily the plasma density. In these conditions, the transmission measurement results in a direct determination of the electronic density with an optimum accuracy better than ~15% in the 10^{23} cm^{-3} range.

In Fig. 3, we display the evolution of the measured transmission of both harmonics (H19 and H21) as a function of the delay with the main pump beam. The transmitted signal for both harmonics corresponds to the same laser shot. The shot to shot stability of the harmonics signal is better than 5% and the experimental points are obtained

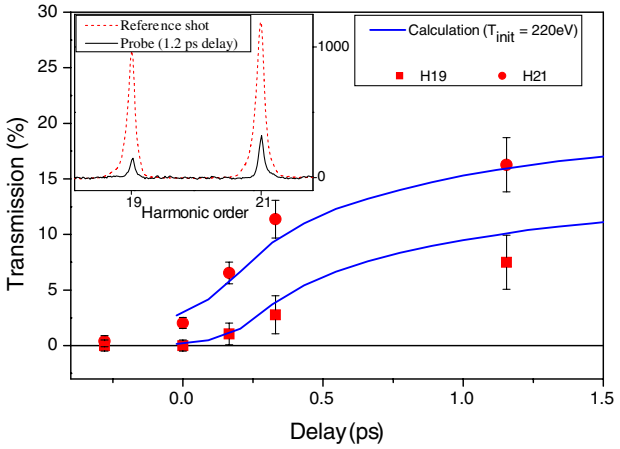

FIG. 3 (color online). Temporal evolution of the transmission of H19 and H21 through the plasma. Full lines: calculation. Inset: respective harmonic spectra for both harmonics for two shots: one without a target (reference) and for a 1.2 ps delay between the pump and the probe (arbitrary units).

by the integration of the spectra shown in the inset of Fig. 3. After each shot, a reference signal is recorded through the exploded foil. The transmission is then calculated as the ratio of the signal over the reference. The first shot (approximately 250 fs before the interaction of the pump with the target) confirms the results presented in the first part of the article: with the PM, the foil is intact, the prepulse-free pump beam interacts hence with a solid density target. The second shot (which establishes more precisely the zero delay for plasma expansion), represents in fact exactly the situation described above, H21 being weakly (~2%) transmitted while H19 shows no observable transmission. The electronic density is then consequently comprised between 2.9 and 3.5×10^{23} cm^{-3}, consistent with the hypothesis of a fully ionized plasma.

After the creation process of the plasma, namely, after the main pulse (60 fs), the transmission of the harmonics increases because the plasma expansion begins. It becomes subcritical for H19 ($< 2.9 \times 10^{23}$ cm^{-3}) after 200 fs, both density and temperature start to decrease. A qualitative model of the hydrodynamic evolution on the basis of an adiabatic expansion was developed in Ref. [13]: assuming an expansion with increasing plasma size $d = d_0 + vt$, where v is the relative speed between both outer profile edges, $v \lesssim 2(2/\gamma - 1)(\gamma Z k_B T_e/m_i)^{1/2}$ (m_i being the ion mass) the density and the temperature decrease in time like $n_e(t) = n_{e0}[d_0/d(t)]$ and $T_e(t) = T_{e0}[n_e(t)/n_{e0}]^{\gamma-1}$, respectively, with $\gamma = 5/3$. An estimate for the light transmission T in a homogeneous foil of size d can be computed using Fresnel's formula for the reflectivity R, giving $T = (1 - R)^2 \exp(-\kappa d)$, where $\kappa = \kappa(T_e, n_e)$ denotes the extinction coefficient. We have opted, however, for a more accurate description of the time evolution of the target by computing the expansion with a one-dimensional hydrodynamic code. Furthermore, the light transmission of both harmonics is computed by simultaneously solving the Helmholtz equation (assuming that the light refraction existing even in the UV region of the spectra is the same for both harmonics). Indeed, with a thickness of a few hundred nanometers and a radial extension of tens of microns, it is reasonable to infer an expansion orthogonal to the surface justifying a one-dimensional simulation. The code hence describes the adiabatic rarefaction propagating into the bulk of an initially almost boxlike shaped density profile, and thus describes properly the early kinetics, and follows the expansion afterwards. The temperature and density profiles inside the bulk are assumed to be uniform initially, which is reasonable for such ultrathin foils. We have for simplicity assumed an ideal gas equation of state (EOS), disregarding heat transport, which is consistent with an adiabatic model.

For the solution of the Helmholtz equation for s-polarized light, we use the Drude model in order to compute the refractive index in which the electron-ion collision frequency ν_{ei} is required. The value of

ν_{ei} is calculated with Spitzer's formula, given by $\nu_{ei}[s^{-1}] = 2.9 \times 10^{-6} Z^2 n_i\ (\mathrm{cm}^{-3}) T_{e,\mathrm{eV}}^{-3/2} \ln\Lambda$, with $\ln\Lambda$ being the Coulomb logarithm [18]. The initial electron density is taken as $3.1 \times 10^{23}\ \mathrm{cm}^{-3}$, while the value of T_{e0} is the only variable allowing to "adjust" the simulation to the experimental data (besides the uncertainty of the onset of the rarefaction from the bulk target, assumed to be of the order of 30–50 fs).

The results are shown in Fig. 3, where the best fit is obtained for an initial temperature of 220 eV with an uncertainty of ± 20 eV (deduced from the spread of the simulation results staying inside the experimental error bars), i.e., better than 15%. We hence observe a very good agreement between experimental data and simulations. The temperature is naturally higher than those seen in Ref. [13] performed at lower intensity and in the same range than previewed in the simulations of Ref. [19] for intensities $\sim 10^{17}\ \mathrm{W/cm}^2$ at normal incidence and somewhat different material conditions (aluminum foil).

The assumption of an ideal gas EOS in the simulations justifies itself by the good agreement with the experimental results and the sufficiently high temperature deduced. We have also checked that it is legitimate to neglect radiative recombination as well as three-body collisions, and hence to consider $Z(= 8)$ to be constant over the 1.5 ps range after the main laser pulse. From the simulation we see that after 1.5 ps, the electron density has dropped from $3.1 \times 10^{23}\ \mathrm{cm}^{-3}$ to $5 \times 10^{22}\ \mathrm{cm}^{-3}$ and the electron temperature from 220 to 65 eV, sufficiently above the Fermi energy ($E_F \simeq 16$ eV). Under these conditions the plasma proves to be on the lower boundary of an almost ideal state, moderately coupled, and weakly degenerate: the coupling coefficient, $\Gamma = Z^2 e^2 n_i^{1/3}/(4\pi\epsilon_0 k_B T_{e0})$ is of the order of $\Gamma \sim 1$, and the degeneracy parameter $k_B T_{e0}/E_F \gtrsim 10$. We find that under such hot and dense plasma conditions where degeneracy and coupling effects are marginal, Spitzer's formula within the Drude model describes quite reliably the matter dynamics (we checked that degeneracy corrections to ν_{ei} do not cause significant change). No extra absorption processes (e.g., ionization or bound-bound or free-free transitions) contribute significantly to the absorption as already seen in [13].

In conclusion, we have demonstrated that the technique based on high-order harmonics generation probe beams is suitable to probe overdense plasmas, in particular, over short time scales with a 100 fs temporal resolution. Under our laser conditions, and, in particular, thanks to the "plasma mirror," we succeeded in accessing an almost ideal plasma state at solid density and a temperature of about 220 eV which does not show expansion until the end of the laser pulse. The temperature, deduced from the hydrosimulations, is estimated to be precise within an error of $\sim 15\%$, as well as the electronic density. The plasma produced in this work originated from an ultrathin foil irradiated with an ultra high intensity cleaned laser pulse. However, we believe that this technique could be used to probe any laser-produced plasma for applications in ignition problems, highly correlated systems, or intense XUV produced plasma, in the "hot and dense" matter state, still experimentally hardly accessible by other means.

This work was supported by the European Communities under the contract of Association between EURATOM and CEA within the framework of the European Fusion Program. The views and opinions expressed herein do not necessarily reflect those of the European Commission.

[1] F. Brunel, Phys. Rev. Lett. **59**, 52 (1987).
[2] P. Gibbon and E. Förster, Plasma Phys. Controlled Fusion **38**, 769 (1996).
[3] D. Umstadter, J. Phys. D: Appl. Phys. **36**, R151 (2003).
[4] D. Giulietti *et al.*, Phys. Rev. Lett. **79**, 3194 (1997), and references therein.
[5] A. Pukhov, Phys. Rev. Lett. **86**, 3562 (2001).
[6] A. Zhidkov, A. Sasaki, and T. Tajima, Phys. Rev. E **61**, R2224 (2000).
[7] A. Maksimchuk, S. Gu, K. Flippo, D. Umstadter, and V. Y. Bychenkov, Phys. Rev. Lett. **84**, 4108 (2000).
[8] J. C. Moreno, C. A. Back, R. C. Cauble, J. A. Koch, and R. W. Lee, Phys. Rev. E **51**, 4897 (1995).
[9] J. C. Kieffer, Z. Jiang, A. Ikhlef, C. Y. Cote, and O. Peyrusse, J. Opt. Soc. Am. B **13**, 132 (1996).
[10] J. Workman *et al.*, Phys. Rev. Lett. **75**, 2324 (1995).
[11] R. F. Smith *et al.*, Phys. Rev. Lett. **89**, 065004 (2002).
[12] P. Salières, A. L'Huillier, Ph. Antoine, and M. Lewenstein, Adv. At. Mol. Opt. Phys. **41**, 83 (1999).
[13] W. Theobald, R. Hassner, C. Wulker, and R. Sauerbrey, Phys. Rev. Lett. **77**, 298 (1996); W. Theobald *et al.*, Phys. Rev. E **59**, 3544 (1999).
[14] H. C. Kapteyn, M. Murnane, A. Szoke, and R. W. Falcone, Opt. Lett. **16**, 490 (1991).
[15] G. Doumy *et al.*, Phys. Rev. E **69**, 026402 (2004).
[16] P. Monot *et al.*, Opt. Lett. **29**, 893 (2004).
[17] K. B. Wharton *et al.*, Phys. Rev. E **64**, 025401(R) (2001).
[18] S. Atzeni and J. Meyer-ter-Vehn, *The Physics of Inertial Fusion* (Clarendon, Oxford 2004).
[19] K. Eidmann, J. Meyer-ter-Vehn, Th. Schlegel, and S. Hüller, Phys. Rev. E **62**, 1202 (2000).